HHS Public Access

Author manuscript

Exp Physiol. Author manuscript; available in PMC 2017 December 06.

Published in final edited form as:

Exp Physiol. 2016 September 01; 101(9): 1206–1217. doi:10.1113/EP085697.

Simultaneous Anterior and Posterior Serosal Mapping of Gastric Slow Wave Dysrhythmias Induced by Vasopressin

Peng Du[1], **Greg O'Grady**[1,2], **Niranchan Paskaranandavadivel**[1], **Shou-jiang Tang**[3], **Thomas Abell**[4], and **Leo K Cheng**[1,5]

[1] Auckland Bioengineering Institute, University of Auckland, New Zealand [2] Department of Surgery, University of Auckland, New Zealand [3] University of Mississippi Medical Center, Jackson, MS, USA [4] University of Louisville, Louisville, KY, USA [5] Department of Surgery, Vanderbilt University, Nashville, TN, USA

Abstract

Background—High-resolution (HR) mapping enables mechanistic insights into gastric slow wave dysrhythmias and is now achieving clinical translation. However, previous studies have focused mainly on dysrhythmias occurring on the anterior gastric wall. The present study simultaneously mapped the anterior and posterior gastric serosa during episodes of dysrhythmias induced by vasopressin to aid understanding of dysrhythmia initiation, maintenance and termination..

Methods—HR mapping (8×16 electrodes on each serosa; 20-74 cm^2) was performed in anesthetized subjects. Baseline recordings (21±8 min) were followed by intravenous vasopressin infusion (0.1-0.5 IU/mL at 60-190 mL/hour) and further recordings (22±13 min). Slow wave activation maps, amplitudes, velocity, interval, and frequency were calculated, and differences compared between baseline and post-infusion.

Results—All subjects demonstrated and increased prevalence of dysrhythmic events following infusion of vasopressin (17% vs 51%).Both amplitude and velocity demonstrated significant differences (baseline vs. post-infusion: 3.6 vs. 2.2 mV; 7.7 vs. 6.5 mm s^{-1}; $P < 0.05$ for both). Dysrhythmias occurred simultaneously or independently on anterior and posterior serosa, and then

Address for Correspondence Dr Peng Du, Auckland Bioengineering Institute, University of Auckland, Private Bag 92019, Auckland 1142, New Zealand. peng.du@auckland.ac.nz.

Author Contributions

PD performed data processing, analysis; NP was responsible signal processing; SJT, TA, GOG, LKC designed the experimental set and obtained experimental data. All authors, PD, GOG, NP, SJT, TA and LKC were involved in the interpretation, writing and approval of the manuscript.

Disclosures

Authors PD, GOG, NP and LKC hold intellectual property interests in the field of gastrointestinal electrophysiology mapping and are shareholders in FlexiMap. TLA is a former licensor, consultant, and investigator for Medtronic.

Supporting Information

Animation1_baseline.mp4 – an example baseline recording
Animation2_rotor.mp4 – rotor
Animation3_retrograde.mp4 – retrograde propagation
Animation4_posterior.mp4 –dysrhythmias in posterior serosa
Animation5_base_dysrhythmias.mp4 – spontaneous dysrhythmias during baseline recording

interacted according to frequency dynamics. A number of persistent dysrhythmias were compared, including: ectopic activation (n=2 subjects), conduction block (n=1), rotor (n=2), retrograde (n=3), collision/merge of wavefronts (n=2).

Conclusions—Infusion of vasopressin induces gastric dysrhythmias, which occurred across a heterogeneous range of frequencies and patterns. The results demonstrated that different classes of gastric dysrhythmias may arise simultaneously or independently in one or both surfaces of the serosa, then interact according to their relative frequencies. These results will help inform clinical dysrhythmia interpretations.

Keywords

High-resolution mapping; interstitial cells of Cajal; gastric electrical activity; gastric dysrhythmias

Introduction

Gastric motility is regulated by several integrated mechanisms, including electrical slow waves generated by the interstitial cells of Cajal (ICC) (Huizinga & Lammers, 2009). In recent years, high-resolution (HR; multi-electrode) mapping has become a prominent technique for quantifying slow wave behaviors, having been applied to clarify normal gastric conduction patterns in large animal models (Lammers *et al.*, 2009; O'Grady *et al.*, 2010), and to spatially define and classify gastric dysrhythmias associated with functional motility diseases (O'Grady *et al.*, 2012*a*; Angeli *et al.*, 2015).

HR mapping studies have shown that normal gastric slow waves form an organized ring-shaped wavefront propagating distally towards the pylorus, with multiple wavefronts propagating simultaneously (Lammers *et al.*, 2009; Egbuji *et al.*, 2010; O'Grady *et al.*, 2010). Gastric dysrhythmias are disruptions to the normal pattern, occurring as either abnormalities of initiation, e.g., stable or unstable ectopic events, or abnormalities of conduction, e.g., conduction blocks, and rotor, as well as frequency disturbances, i.e., tachygastria and bradygastria (Lammers, 2013). Two recent intra-operative HR mapping studies have related gastric dysrhythmias to motility disorders, in gastroparesis and chronic unexplained nausea and vomiting (O'Grady *et al.*, 2012; Angeli *et al.*, 2015), and dysrhythmias may also play a role in functional dyspepsia (Lin & Chen, 2001). These studies have shown the potential of HR mapping as a clinically important tool to define the underlying pathophysiology of gastric motility disorders and to aid in diagnosis (O'Grady *et al.*, 2014).

To date, most HR mapping studies in large animal models have been largely conducted in subjects with dysrhythmias occurring spontaneously (O'Grady *et al.*, 2011), or in the context of opioid analgesic use (Lammers *et al.*, 2008). In sparse electrode studies, drug-induced gastric dysrhythmias have been induced via administration of several agents, including glucagon (Abell & Malagelada, 1985; Xu & Chen, 2007; Bradshaw *et al.*, 2007), vasopressin (Chen *et al.*, 2003; Qian *et al.*, 2003), epinephrine (Kim *et al.*, 1989), and as a response to chemotherapy agents (Yu *et al.*, 2009). In general, there were two limitations with the previous studies using sparse electrodes: First, these studies generally focused on changes in the frequency of gastric slow waves (Koch, 2014), rather than also incorporating

spatial patterns of dysrhythmia (Koch, 2011); Second, in a majority of cases only the anterior gastric serosa was monitored, and it was unclear how the slow waves on the posterior serosa developed during an episode of gastric dysrhythmia on the anterior serosa.

There were two aims to this study. The first aim was to re-evaluate a reliable drug-induced large animal model of gastric dysrhythmias, i.e., vasopressin, using HR mapping, as a basis for repeatable mapping studies and intervention trials. The second aim was to assess how gastric dysrhythmias develop and interact simultaneously over both the anterior and posterior gastric surfaces. To date, most slow wave recordings have been focused only on the anterior gastric serosa (Lin & Chen, 2001; Lammers *et al.*, 2008; Angeli *et al.*, 2015), whereas this study involved a comparative analysis on both serosal surfaces. Furthermore, there is a need to better understand how gastric dysrhythmias spatially evolve and interact over the entire circumference of the stomach, in order to accurately interpret the consequences and dynamics of dysrhythmic patterns on whole-organ slow wave activity.

Materials and Methods

Ethical Approval

Ethical approval was granted the University of Mississippi Medical Center Institutional Animal Care and Use Committee (IACUC). Experiments strictly adhered to the guidelines of the IACUC. Recording protocols were similar to previously described HR mapping studies (Egbuji *et al.*, 2010; Angeli *et al.*, 2013). All studies were conducted under general anesthesia, with continuous monitoring of vital signs. The induction protocols included telezol (4.4 mg/kg), domitor (0.08 mg/kg), burophanol (0.2 mg/kg) and ketamine (10 mg/kg) and maintenance anesthesia was with isoflurane (1-3%) via IV. Anesthetic monitoring included HR, RR, SpO2. Attention is given to the degree of muscle tone and any resistance to the ventilator. A midline laparotomy was performed to expose the stomach, and the wound edges were approximated whenever possible to prevent gastric serosa from cooling and drying. At the conclusion of the experiment, the subject was euthanized with an IC injection of concentrated pentobarbital to induce cardiac arrest, while under general anesthesia.

Animal Preparation and Recordings

Experiments were performed on five hound dogs (20-23 kg). To date porcine and canine models are the two large monogastric animal models that have been primarily used for gastric dysrhythmia investigations (Lammers *et al.*, 2009; Egbuji *et al.*, 2010). Comparing the porcine model, the canine stomach has less quiescent area and the similar rapid transition of slow waves in the antrum that has been identified in the human stomach (O'Grady *et al.*, 2010). Furthermore, vasopressin has also been previously applied in canine subjects to invoke gastric dysrhythmias (Chen *et al.*, 2003; Qian *et al.*, 2003). Therefore the canine model was chosen as the preferred animal model in this study.

Validated flexible printed circuit (FPC) recording arrays were used for mapping (inter-electrode spacing: 4 or 7.62 mm) (Du *et al.*, 2009). The electrode arrays were arranged into two ‘patches’, with each patch containing 128 electrodes in a 16×8 configuration (a total of

256 electrodes), as shown in Figure 1. An anterior serosal patch was positioned over the antrum or lower corpus, and the second patch was placed on the posterior serosa in an approximately mirrored position. Attention was paid to ensure that the placements of the electrode arrays were reasonably consistent relative to the major anatomical landmarks, such as the incisura angularis and pylorus of the stomach, in a mirrored fashion between the two serosa. Two different electrode arrays (coverage: 20 or 74 cm^2 for each patch) were used to ensure that proportion of coverage between subjects was relatively consistent, as shown in Figure 2. Warm saline-soaked gauze packs were gently placed over the electrodes to maintain gentle contact with the serosa. Signals were acquired at 512 Hz using a passive recording system (BioSemi, the Netherlands), with the reference lead placed on the hind-leg.

For each subject, a baseline recording was conducted for approximately 21±8 min following an initial 10 min stabilization period after the incision. Vasopressin was administered intravenously at a dosage of 0.1-0.5 IU/mL; infusion: 60-190 mL/hr. Gastric slow waves were recorded over an average duration of 22±13 min following infusion.

Data Processing

All data analysis was performed in the Gastrointestinal Electrical Mapping Suite (GEMS) (Yassi *et al.*, 2012). After down-sampling the data to 30 Hz a Savitzky-Golay filter was applied to the signals to remove high-frequency noise (Paskaranandavadivel *et al.*, 2013). Activation times of slow waves were detected and grouped using established automated algorithms (Erickson *et al.*, 2010, 2011). Manual review was performed for all processed signals. The normal gastric slow wave pattern was defined as regular propagation in the antegrade direction towards the pylorus (Figure 1B, C), whereas dysrhythmic events were defined as deviations of the normal propagation pattern, using criteria proposed in previous large animal studies (Lammers *et al.*, 2008; O'Grady *et al.*, 2011, 2012). Specific definitions of spatial dysrhythmias are listed in Table 1 and their hierarchy is illustrated in Figure 1D. Previous studies have described a major transition in these slow wave characteristics to occur in the distal antrum (Lammers *et al.*, 2009; O'Grady *et al.*, 2010), and therefore all post-infusion recordings were compared specifically to the baseline recordings in each subject without moving the electrode arrays.

The dysrhythmias formed patterns with distinct circumferential and longitudinal components, e.g., ectopic activity, the orthogonal velocity components were decomposed based on the velocity vector at the same electrode in the baseline recording, as previously described (Du *et al.*, 2011) . An “anisotropic ratio” (AR), i.e., circumferential/longitudinal velocity was calculated for the dysrhythmic episode (Du *et al.*, 2015).

Statistical Methods

Measured amplitude (mV), velocity (mm s^{-1}), interval (s), and frequency (cycles/min) values were defined for all detected slow wave events. The paired Student's t-test was used to test statistical differences occurring pre and post infusion of vasopressin (significance threshold $P<0.05$). Mean values with standard deviation (SD) are reported as appropriate.

Results

Baseline Recordings

On average 67±6 cycles of baseline slow waves and 70±28 cycles of post-infusion slow waves per subject were analyzed. Gastric slow waves were shown to propagate simultaneously across both the anterior and posterior serosa of the stomach in all five subjects. During normal propagation sequences, the independently mapped propagation patterns on the anterior and posterior serosa mirrored each other in all subjects, when accounting for minor offsets in the relative electrode positions (Figure 2).

Due to the differences in orientation and coverage of electrodes, some studies recorded mostly antral slow waves, e.g., Figure 2A, while others recorded a combination of corpus and antral slow waves, e.g., Figure 2C. As per the methods, these data were compared differently. The average amplitude, velocity, interval, and frequency of gastric slow waves during baseline recordings are reported in Table 2.

During baseline recordings, two out of the five subjects showed brief periods of spontaneously occurring dysrhythmias. There were multiple episodes of brief (54 - 56 s) dysrhythmias, which also exhibited dynamic spatiotemporal propagations, comprising re-entry and retrograde propagations in one subject, and stable retrograde propagation in the other subject. Overall, dysrhythmic episodes accounted for 17±11% of the total number of cycles of baseline recordings.

Post-Vasopressin Recordings

A number of spatial gastric dysrhythmias were identified following vasopressin infusion. On average, across the five subjects, there was an increase in dysrhythmias from 17% in baseline to 51% in post-infusion recordings. The rate and range of dysrhythmic episodes were highly heterogeneous following vasopressin infusion, occurring in on average 51±19% of the episodes analyzed across the five subjects (Table 2).

Significant reductions in both the amplitude and velocity of slow waves were observed following vasopressin infusion (Table 2), with highly heterogeneous responses within and between subjects. A number of typical dysrhythmia classes were observed, which included: ectopic activity (n=2 subjects), conduction block (n=5), rotor (n=2), retrograde propagation (n=3), merge/collision (n=2). Across this range of dysrhythmias, substantial variation in frequencies were observed (2.7-4.7 cycles/min). One subject demonstrated an overall reduction in frequency (baseline vs infusion: 3.8 ± 0.4 vs 2.8 ± 0.5 cycles/min; $P < 0.05$), partly due to a long period of quiescence (~200 s) following vasopressin infusion. In general, the subjects demonstrated relatively elevated frequencies compared to their baseline values.

In-depth analyses were undertaken for representative cases of each of the major identified dysrhythmia classes to compare and demonstrate propagation patterns across the anterior and posterior serosal surfaces, as presented in the following sections.

Posterior Rotor—Rotor was observed in two subjects, occurring on either the anterior or posterior serosa, but never simultaneous over both. An example of rotor shown in Figure 3, which was located on the posterior serosal surface. The rotor was defined as rotation of slow wave around a “core” in a single direction (Lammers *et al.*, 2005), whereas previous studies have also identified double rotors in the stomach, which was also defined as figure-of-eight reentry (Du *et al.*, 2014). During the rotor reentry, the anterior serosal surface showed rapid circumferential propagation, giving rise to both antegrade and retrograde wavefronts. The frequency of the rotor was elevated relative to the baseline recordings in this subject (3.6±0.4 vs 2.7±0.5 cycles/min; $P < 0.05$). The duration of the rotor lasted approximately 197 s.

The diameter of the rotor around the location of the selected electrograms in Figure 3 was approximately 8 mm, which gave a circumference of 25 mm (8π). The average interval of the rotor was 15±4 s, giving an average velocity of 1.9±0.3 mm s^{-1} in the direction of the rotor, which was substantially slower than the baseline velocity in the same subject of 8.6±1.2 mm s^{-1} ($P < 0.05$). The average AR of the rotor of was 2.0±0.9.

Uncoupled Retrograde Propagation with Collision—Figure 4 demonstrates an example of retrograde activity on the distal anterior serosal field, with quiescence of the majority of the proximal field, which had demonstrated regular activity during the baseline recordings (Figure 2A). Retrograde activity also occurred over the posterior surface, but with co-existence of antegrade activity, resulting in slow-wave collision. Overall, retrograde propagations occurred in 3 subjects following vasopressin infusion, resulting in collisions of wavefronts in 2 subjects.

In the example case in Figure 4, both retrograde activities in the anterior and posterior serosal surfaces occurred at an identical frequency of 0.8±0.2 cycles/min ($P = 0.16$), indicating likely a common ectopic origin. The antegrade activity at the posterior serosal surface occurred at a frequency of 2.3±0.5 cycles/min, which was lower than the baseline frequency in the same subject (3.8±0.4 cycles/min; $P < 0.05$). The frequency mismatch between the antegrade and retrograde activities resulted in a collision between the two wavefronts in wave 1 and 2, and a functional block in wave 3 even in the absence of a retrograde activity in both serosal surfaces, i.e., no wave in the distal region of the maps, as shown in Figure 4 (Wave 3). The velocity during this period was also lower than the baseline velocity (baseline vs dysrhythmia: 7.8 ± 3.7 vs 3.3 ± 0.8 mm s^{-1}; $P < 0.05$).

Frequency uncoupled dysrhythmias restricted to one serosa—Uncoupled activity could also be restricted to one serosal surface without perturbation to the normal activity occurring at the other surface, which was observed in 2 subjects. An example of this type of spatial dysrhythmia is shown in Figure 5, where the electrograms in electrodes 1-4 in the posterior surface occurred at a different frequency than the remainder of the mapped field (3.1±0.1 vs 5.9±0.2 cycles/min; $P < 0.05$), during the 60 s period shown. Overall, the main antegrade activity was also higher than the baseline frequency recorded from the same subject (baseline vs post-infusion; 3.6 ± 0.2 vs 4.0 ± 0.6 cycles/min; p-value < 0.05). However, unlike the uncoupled retrograde activity shown in Figure 4, which resulted in collision or conduction block, the uncoupled antegrade activity merged with the normal

wavefront as a single coherent wavefront in the posterior serosal surface at alternating cycles (Figure 5A). Alternatively, this could be seen as a 2:1 entrainment of two competing pacemakers in the posterior serosa (O'Grady *et al.*, 2011).

In addition, the average velocity of the uncoupled antegrade activity was 4.8 ± 0.7 mm s^{-1}, which was slower than the main antegrade velocity (8.6 ± 0.4 mm s^{-1}; $P < 0.05$).

Discussion

This study utilized HR mapping to spatiotemporally evaluate gastric slow wave dysrhythmias across both the anterior and posterior gastric serosal surfaces following infusion of vasopressin in five dog subjects. The main findings were: i) the subjects developed a substantial increased frequency of gastric dysrhythmias following infusion of vasopressin, and of several different classes; (ii) spatial dysrhythmias could occur simultaneously or independently in both or just one serosal surfaces, with propagation interactions between waves determined by relative frequencies; (iii) most dysrhythmias could occur across a range of frequencies, but rotor was always associated with a relatively elevated frequency.

The advent of HR mapping offers a refined definition and categorization of gastric dysrhythmias (Lammers *et al.*, 2008; O'Grady *et al.*, 2011, 2012; Angeli *et al.*, 2015), yet very few studies have previously offered simultaneous HR data on gastric slow waves from both the anterior and posterior serosa. One of the key observations from this study was the independent onset of dysrhythmias in the anterior and posterior surfaces over consecutive cycles of gastric slow waves, as demonstrated in example Figures 3 and 5. Previous studies mostly assumed that slow waves propagated symmetrically in the anterior and posterior serosa, which is true for normal activation (Figure 1). The importance of this finding is twofold: First, from a physiological viewpoint, it is clear that the origin of gastric dysrhythmias could be originate from either serosa, and could meander dynamically. Therefore, spatial dysrhythmias in the anterior serosa could trace their origin to the posterior serosa, by propagating across the greater curvature, as shown in Figure 3, or vice-versa. This finding could mean that events previously defined as ectopic activation at the greater curvature in HR studies (Lammers *et al.*, 2008; O'Grady *et al.*, 2012; Angeli *et al.*, 2015), may have actually been secondary to a unidentified dysrhythmic event occurring on the posterior stomach, away from the mapped field. Second, it is clear that from a therapeutic perspective, optimal targeting of ectopic pacemakers and complete elimination of dysrhythmias can only be ensured by monitoring both serosa.

The rotor reported in this study (Figure 3) was associated with regular relative elevated frequency compared to the baseline frequency recorded from the same subject (4.3 ± 0.1 vs 3.6 ± 0.4 cycles/min), which was consistent with previously reported rotor in the canine stomach (Lammers *et al.*, 2008). However, a significant difference between the present the study and the previous HR mapping study was in the absolute values of tachygastria and baseline frequency during rotor (14.7 ± 7.4 vs 4.9 ± 0.6 cycles/min), as reported previously (Lammers *et al.*, 2008). The discrepancy could potentially be explained by the specific dysrhythmic effect of vasopressin, which often induced bradygastria in this and other studies

(Xu *et al.*, 2005; Song *et al.*, 2006), or possibly by differences in breed (hound vs. beagle), and / or the fact the rotor persisted up to 197 s. The implication of the more persistent rotor but with less pronounced elevation in frequency could lead to a larger 'excitable gap', allowing for the gastric tissue to completely recover before it is re-excited by the re-entrant wavefront, or for another propagating event to interrupt and terminate the rotor. A complementary finding was reported in a HR mapping study of a stable porcine gastric rotor (4.1 ± 0.2 vs 3.2 ± 0.2 cycles/min) (O'Grady *et al.*, 2011), which was close to the frequencies observed in this study.

Previous studies have also reported 'uncoupling' of slow wave activity to be associated with gastric dysrhythmias, including through stable or unstable ectopic pacemaking as a mechanism for perpetuating ongoing cycles of uncoupled activity (Coleski & Hasler, 2009; Bradshaw *et al.*, 2009). The present study demonstrated for the first time that uncoupling could also occur in both serosal surfaces together, or on either independently (e.g. Figures 4 and 5). It is worth comparing the difference between the uncoupling result and a previous study using sparse electrodes (Qian *et al.*, 2003), which demonstrated tachygastria originating from ectopic activity in the antrum and bradygastria in the corpus. Such a mixed brady-tachy pattern could be explained by various scenarios. For example, a likely explanation for the bradygastric retrograde propagation reported in the present study is the lower intrinsic frequencies of the ICC in the antrum region, as expressed during ectopic pacemaking (Kelly & Code, 1971; Sarna *et al.*, 1972). On the other hand, rotor located in the antrum could also lead to a relative elevated frequency of dysrhythmias originating from the antrum (Lammers *et al.*, 2008), as was also observed in the present study (Figure 3).

Changes in gastric slow wave frequency have been the main method for evaluating gastric dysrhythmia following drug induction in previous studies (Qian *et al.*, 2003; Xu & Chen, 2007; Yu *et al.*, 2009). Both the present study and other previous HR mapping studies have demonstrated that while many gastric dysrhythmias are associated with a change in slow wave frequency (Lammers *et al.*, 2008; O'Grady *et al.*, 2011), frequency alone cannot accurately predict the occurrence, location and type of the dysrhythmias occurring in the stomach, many of which may also occur at normal frequency in some species including humans (O'Grady *et al.*, 2012; Angeli *et al.*, 2015). Detection of the spatial details of these dysrhythmias is important for understanding the potential mechanisms of the dysrhythmias, as highlighted by the bradygastria associated with retrograde propagation (Figure 4). Furthermore, a brief period of regular or irregular change in frequency may be present amid a long period of normal frequency activity, so the overall frequency following an intervention may not be significantly different from the baseline frequency. Therefore, a fine temporal-solution method such as using a shifting-window (Lin & Chen, 2001), or beat-to-beat interval (Lammers *et al.*, 2008), may be used to calculate frequency rather than using a spectral analysis on the entire segment of recording.

There are a number of limitations in the present study. First, the baseline data included significant inter-subject variations (Figure 2), with two out of five subjects also showing brief periods of spontaneous dysrhythmias (Animation 5, with direction of normal propagation restored after approximately 200 s), which was in agreement with a previously study under similar experimental conditions (Lammers *et al.*, 2008). Second, the recording

coverage of the electrode arrays were limited in some subjects, e.g., Figure 4, which could be improved by using near real-time detection algorithms to determine adequate contact and coverage before recording (Bull *et al.*, 2014). However, care should be taken to distinguish the normal 'electrically quiescent' regions in the stomach (Lammers *et al.*, 2009; Egbuji *et al.*, 2010; O'Grady *et al.*, 2010), from conduction block during dysrhythmia (Figure 4). In addition, there were some minor differences in array alignment noted between the anterior and posterior curvature, which were exaggerated in some cases by the rapid transition in slow waves normally occurring in the distal canine stomach (Lammers *et al.*, 2009). However, imperfect alignment did not contribute to the observed heterogeneity of the mapping data, which was due to the inconsistent and variable nature of the dysrhythmias. In the future, a subject-specific method of registering the electrode arrays could be investigated, such as from pre-operative MRI or CT. Lastly, the assessment of gastric function using HR mapping was limited to extracellular electrical mapping in the fasted state under general anesthesia, whereas previous studies using alternative methods have demonstrated chronic recordings of gastric slow waves and motility (Ver Donck *et al.*, 2006; Yu *et al.*, 2009; Song & Chen, 2011).

In summary, the present study provides the first attempt to quantitatively analyze the onset of gastric dysrhythmias in high spatiotemporal details following infusion of vasopressin. A significant increase in the episodes of spatial dysrhythmias were identified following infusion of vasopressin, and events were characterized and compared across the gastric curvatures. The source of dysrhythmias could be traced to either anterior or posterior surfaces, which suggests a better representation of the organ level dysrhythmias could be gained by increasing the coverage of recording while maintaining the spatial resolution. It would be also valuable in the future to map around the full circumference of human gastric dysrhythmias using similar methods to the current study, as well as potential chronic studies of the effects of gastric distention on slow waves. Elimination and/or management of these dysrhythmias has potential to provide a novel avenue of treatment for the refractory nausea and vomiting symptoms commonly associated with these diseases (O'Grady *et al.*, 2012, 2014; Angeli *et al.*, 2015).

Supplementary Material

Refer to Web version on PubMed Central for supplementary material.

Acknowledgements

This work and authors were funded by grants from the National Institute of Health (R01 DK64775), the New Zealand (NZ) Health Research Council, and the NZ MedTech CoRE. PD is supported by the Rutherford Foundation Trust, and a Marsden Fast-Start Grant by the Royal Society of NZ.

References

Abell TL, Malagelada JR. Glucagon-evoked gastric dysrhythmias in humans shown by an improved electrogastrographic technique. Gastroenterology. 1985; 88:1932–1940. [PubMed: 3996846]

Angeli TR, Cheng LK, Du P, Wang TH-H, Bernard CE, Vannucchi M-G, Faussone-Pellegrini MS, Lahr C, Vather R, Windsor JA, Farrugia G, Abell TL, O'Grady G. Loss of Interstitial Cells of Cajal

and Patterns of Gastric Dysrhythmia in Patients With Chronic Unexplained Nausea and Vomiting. Gastroenterology. 2015; 149:56–66. e5. [PubMed: 25863217]

Angeli TR, O'Grady G, Du P, Paskaranandavadivel N, Pullan AJ, Bissett IP, Cheng LK. Circumferential and functional re-entry of in vivo slow-wave activity in the porcine small intestine. Neurogastroenterol Motil. 2013; 25:e304–e314. [PubMed: 23489929]

Bradshaw LA, Irimia A, Sims JA, Richards WO. Biomagnetic signatures of uncoupled gastric musculature. Neurogastroenterol Motil. 2009; 21:778–e50. [PubMed: 19222760]

Bradshaw LA, Sims JA, Richards WO. Noninvasive assessment of the effects of glucagon on the gastric slow wave. Am J Physiol Gastrointest Liver Physiol. 2007; 293:G1029–G1038. [PubMed: 17884978]

Bull SH, O'Grady G, Du P, Cheng LK. A system and method for online high-resolution mapping of gastric slow-wave activity. IEEE Trans Biomed Eng. 2014; 61:2679–2687. [PubMed: 24860024]

Chen JDZ, Qian L, Ouyang H, Yin J. Gastric electrical stimulation with short pulses reduces vomiting but not dysrhythmias in dogs. Gastroenterology. 2003; 124:401–409. [PubMed: 12557146]

Coleski R, Hasler WL. Coupling and propagation of normal and dysrhythmic gastric slow waves during acute hyperglycaemia in healthy humans. Neurogastroenterol Motil. 2009; 21:492–499. e1–e2. [PubMed: 19309443]

Ver Donck L, Lammers WJ, Moreaux B, Smets D, Voeten J, Vekemans J, Schuurkes JA, Coulie B. Mapping slow waves and spikes in chronically instrumented conscious dogs: implantation techniques and recordings. Med Biol Eng Comput. 2006; 44:170–178. [PubMed: 16937158]

Du P, Hameed A, Angeli TR, Lahr C, Abell TL, Cheng LK, O'Grady G. The impact of surgical excisions on human gastric slow wave conduction, defined by high-resolution electrical mapping and in silico modeling. Neurogastroenterol Motil. 2015 DOI: 10.1111/nmo.12637.

Du P, O'Grady G, Egbuji JU, Lammers WJ, Budgett D, Nielsen P, Windsor JA, Pullan AJ, Cheng LK. High-resolution mapping of in vivo gastrointestinal slow wave activity using flexible printed circuit board electrodes: methodology and validation. Ann Biomed Eng. 2009; 37:839–846. [PubMed: 19224368]

Du P, O'Grady G, Paskaranandavadivel N, Angeli TR, Lahr C, Abell TL, Cheng LK, Pullan AJ. Quantification of velocity anisotropy during gastric electrical arrhythmia. Conf Proc . Annu Int Conf IEEE Eng Med Biol Soc IEEE Eng Med Biol Soc Annu Conf. 2011; 2011:4402–4405.

Du P, Paskaranandavadivel N, O'Grady G, Tang SJ, Cheng LK. A Theoretical Analysis of the Initiation, Maintenance and Termination of Gastric Slow Wave Re-entry. J Theor Biol. 2014

Egbuji JU, O'grady G, Du P, Cheng LK, Lammers WJ, Windsor JA, Pullan AJ. Origin, propagation and regional characteristics of porcine gastric slow wave activity determined by high-resolution mapping. Neurogastroenterol Motil. 2010; 22:e292–e300. [PubMed: 20618830]

Erickson JC, O'Grady G, Du P, Egbuji JU, Pullan AJ, Cheng LK. Automated gastric slow wave cycle partitioning and visualization for high-resolution activation time maps. Ann Biomed Eng. 2011; 39:469–483. [PubMed: 20927594]

Erickson JC, O'Grady G, Du P, Obioha C, Qiao W, Richards WO, Bradshaw LA, Pullan AJ, Cheng LK. Falling-edge, variable threshold (FEVT) method for the automated detection of gastric slow wave events in high-resolution serosal electrode recordings. Ann Biomed Eng. 2010; 38:1511–1529. [PubMed: 20024624]

Huizinga JD, Lammers WJ. Gut peristalsis is governed by a multitude of cooperating mechanisms. Am J Physiol Gastrointest Liver Physiol. 2009; 296:G1–G8. [PubMed: 18988693]

Kelly KA, Code CF. Canine gastric pacemaker. Am J Physiol. 1971; 220:112–118. [PubMed: 5538644]

Kim CH, Hanson RB, Abell TL, Malagelada JR. Effect of inhibition of prostaglandin synthesis on epinephrine-induced gastroduodenal electromechanical changes in humans. Mayo Clin Proc. 1989; 64:149–157. [PubMed: 2921874]

Koch KL. The electrifying stomach. Neurogastroenterol Motil. 2011; 23:815–818. [PubMed: 21838727]

Koch KL. Gastric dysrhythmias: a potential objective measure of nausea. Exp brain Res. 2014; 232:2553–2561. [PubMed: 24916149]

Lammers WJ. Arrhythmias in the gut. Neurogastroenterol Motil. 2013; 25:353–357. [PubMed: 23490042]

Lammers WJ, Ver Donck L, Schuurkes JA, Stephen B. Peripheral pacemakers and patterns of slow wave propagation in the canine small intestine in vivo. Can J Physiol Pharmacol. 2005; 83:1031–1043. [PubMed: 16391712]

Lammers WJ, Ver Donck L, Stephen B, Smets D, Schuurkes JA. Focal activities and re-entrant propagations as mechanisms of gastric tachyarrhythmias. Gastroenterology. 2008; 135:1601–1611. [PubMed: 18713627]

Lammers WJ, Ver Donck L, Stephen B, Smets D, Schuurkes JA. Origin and propagation of the slow wave in the canine stomach: the outlines of a gastric conduction system. Am J Physiol Gastrointest Liver Physiol. 2009; 296:G1200–G1210. [PubMed: 19359425]

Lin X, Chen JZ. Abnormal gastric slow waves in patients with functional dyspepsia assessed by multichannel electrogastrography. Am J Physiol Gastrointest Liver Physiol. 2001; 280:G1370–G1375. [PubMed: 11352832]

O'Grady G, Angeli TR, Du P, Lahr C, Lammers WJ, Windsor JA, Abell TL, Farrugia G, Pullan AJ, Cheng LK. Abnormal initiation and conduction of slow-wave activity in gastroparesis, defined by high-resolution electrical mapping. Gastroenterology. 2012; 143:583–589.

O'Grady G, Du P, Cheng LK, Egbuji JU, Lammers WJ, Windsor JA, Pullan AJ. Origin and propagation of human gastric slow-wave activity defined by high-resolution mapping. Am J Physiol Gastrointest Liver Physiol. 2010; 299:G585–G592. [PubMed: 20595620]

O'Grady G, Egbuji JU, Du P, Lammers WJ, Cheng LK, Windsor JA, Pullan AJ. High-resolution spatial analysis of slow wave initiation and conduction in porcine gastric dysrhythmia. Neurogastroenterol Motil. 2011; 23:e345–e355. [PubMed: 21714831]

O'Grady G, Wang TH-H, Du P, Angeli T, Lammers WJEP, Cheng LK. Recent progress in gastric arrhythmia: pathophysiology, clinical significance and future horizons. Clin Exp Pharmacol Physiol. 2014; 41:854–862. [PubMed: 25115692]

Paskaranandavadivel N, O'Grady G, Du P, L KC, Cheng LK. Comparison of filtering methods for extracellular gastric slow wave recordings. Neurogastroenterol Motil. 2013; 25:79–83. [PubMed: 22974243]

Qian LW, Pasricha PJ, Chen JDZ. Origins and patterns of spontaneous and drug-induced canine gastric myoelectrical dysrhythmia. Dig Dis Sci. 2003; 48:508–515. [PubMed: 12757162]

Sarna SK, Daniel EE, Kingma YJ. Effects of partial cuts on gastric electrical control activity and its computer model. Am J Physiol. 1972; 223:332–340. [PubMed: 5046751]

Song G, Hou X, Yang B, Sun Y, Liu J, Qian W, Chen JDZ. Efficacy and efficiency of gastric electrical stimulation with short pulses in the treatment of vasopressin-induced emetic responses in dogs. Neurogastroenterol Motil. 2006; 18:385–391. [PubMed: 16629866]

Song G-Q, Chen JDZ. Gastric electrical stimulation on gastric motility in dogs. Neuromodulation. 2011; 14:271–277. discussion 277. [PubMed: 21992252]

Xu J, Chen JDZ. Effects of cyclooxygenase-2 inhibitor on glucagon-induced delayed gastric emptying and gastric dysrhythmia in dogs. Neurogastroenterol Motil. 2007; 19:144–151. [PubMed: 17244169]

Xu X, Brining DL, Chen JDZ. Effects of vasopressin and long pulse-low frequency gastric electrical stimulation on gastric emptying, gastric and intestinal myoelectrical activity and symptoms in dogs. Neurogastroenterol Motil. 2005; 17:236–244. [PubMed: 15787943]

Yassi R, O'Grady G, Paskaranandavadivel N, Du P, Angeli TR, Pullan AJ, Cheng LK, Erickson JC. The gastrointestinal electrical mapping suite (GEMS): software for analyzing and visualizing high-resolution (multi-electrode) recordings in spatiotemporal detail. BMC Gastroenterol. 2012; 12:60. [PubMed: 22672254]

Yu X, Yang J, Hou X, Zhang K, Qian W, Chen JDZ. Cisplatin-induced gastric dysrhythmia and emesis in dogs and possible role of gastric electrical stimulation. Dig Dis Sci. 2009; 54:922–927. [PubMed: 18754094]

New Findings

- The first comparison of simultaneous high-resolution mapping of anterior and posterior gastric serosa over sustained periods.
- Episodes of spontaneous gastric slow wave dysrhythmias increased significantly following intravenous infusion of vasopressin compared to the baseline state.
- A number of persistent dysrhythmias were defined, including: ectopic activation, conduction block, rotor, retrograde, collision/merge of wavefronts.
- Slow wave dysrhythmias could occur either simultaneously or independently on the anterior and posterior gastric serosa, and interacted depending on activation-repolarization and frequency dynamics.

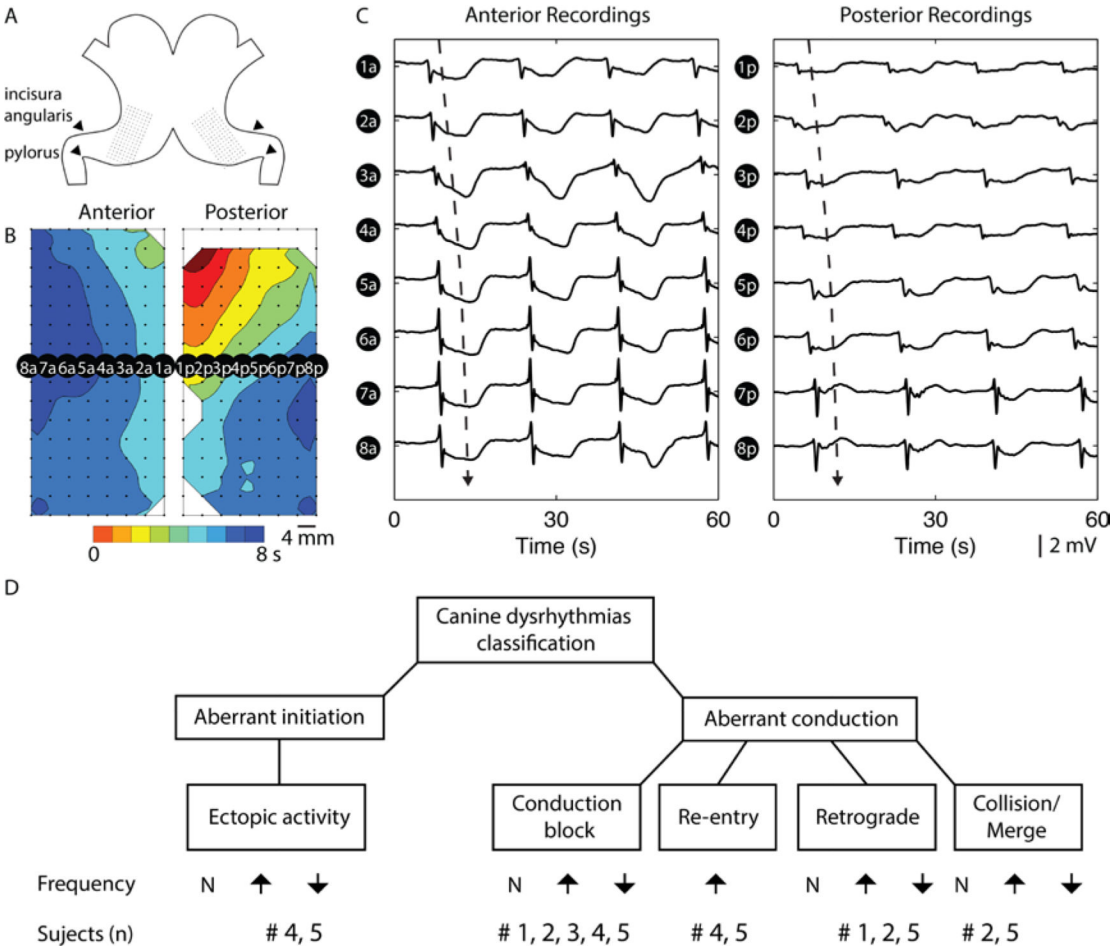

Figure 1.

Setup of high-resolution (HR) electrical mapping of canine stomach. A. Two electrode arrays each containing 128 electrodes arranged in a 16 by 8 configuration was placed on the anterior and posterior serosal surfaces of the stomach, in a mirrored fashion. B. Slow wave recordings were mostly obtained from lower gastric antrum region of the stomach, and reconstructed into activation map of anterior and posterior maps, representing one cycle of slow wave propagation. The red color represents early activation and the blue color represents later activation of slow waves. Each band of color represents an interval of 1 s, i.e., the larger the gap between two consecutive lines (isochrones), the more distance the slow wave propagated over the 1 s interval, therefore the faster the velocity in this region. C. A selection of recordings at 16 electrodes demonstrate the sequential propagation of slow waves (“a” denotes anterior electrodes, and “p” denotes posterior electrodes), with the dashed arrow representing the direction and wave plotted in the activation map in B. D. Classifications of gastric dysrhythmias and summary of subject numbers associated with each dysrhythmias following infusion of vasopressin.

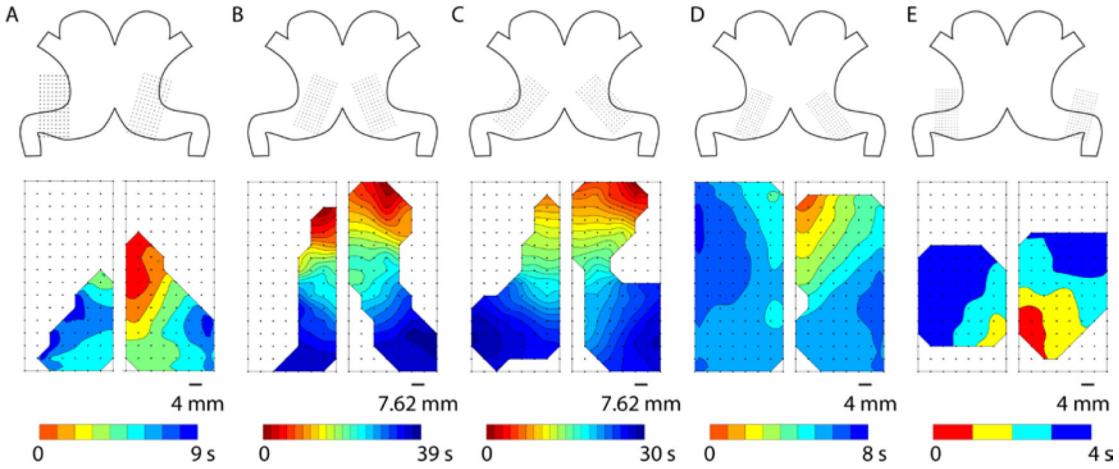

Figure 2.

Example activation times maps of canine gastric slow waves in five subjects (A-E). Top: The orientations and positions of the electrode arrays illustrate the coverage of the mapping fields in each subject. Bottom: Activation times map of a typical cycle of gastric slow waves from each subject, showing approximately simultaneous and antegrade propagation towards the pylorus. Note the larger arrays were used in 2 (B) and 3 (C), resulting in a substantially longer overall activation period (~35 s) and more closely-spaced isochrones (1 s interval in all activation times maps).

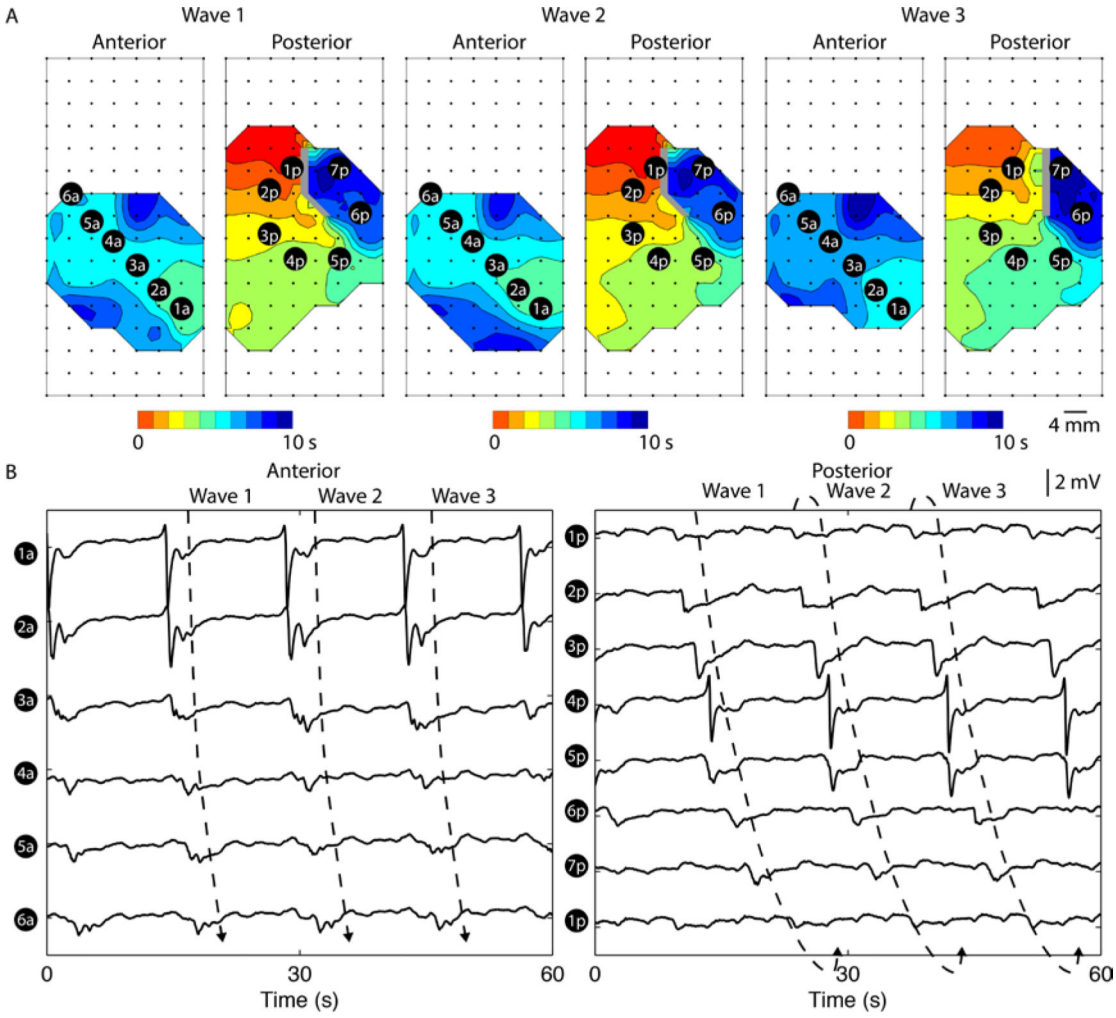

Figure 3.

Canine gastric rotor on the posterior serosal surface of the stomach. A. Three consecutive rotor re-entries over a period of 60 s. Each isochronal band in the activation maps represents an interval of 1 s. Orientations and locations of the electrode arrays were identical to Figure 2E. A rotor in the counter clock-wise direction in the posterior serosal surface was detected. B. Six electrodes (1a-6a) were selected from the anterior serosal surface to demonstrate propagation in the antegrade direction towards the gastric pylorus. Seven electrodes (1p-7p) were selected from the posterior serosal surface in the direction of propagation, with electrode 1p repeated after electrode 7p, to demonstrate re-entry. A single rotor took approximately 15±4 s to complete the re-entrant pathway.

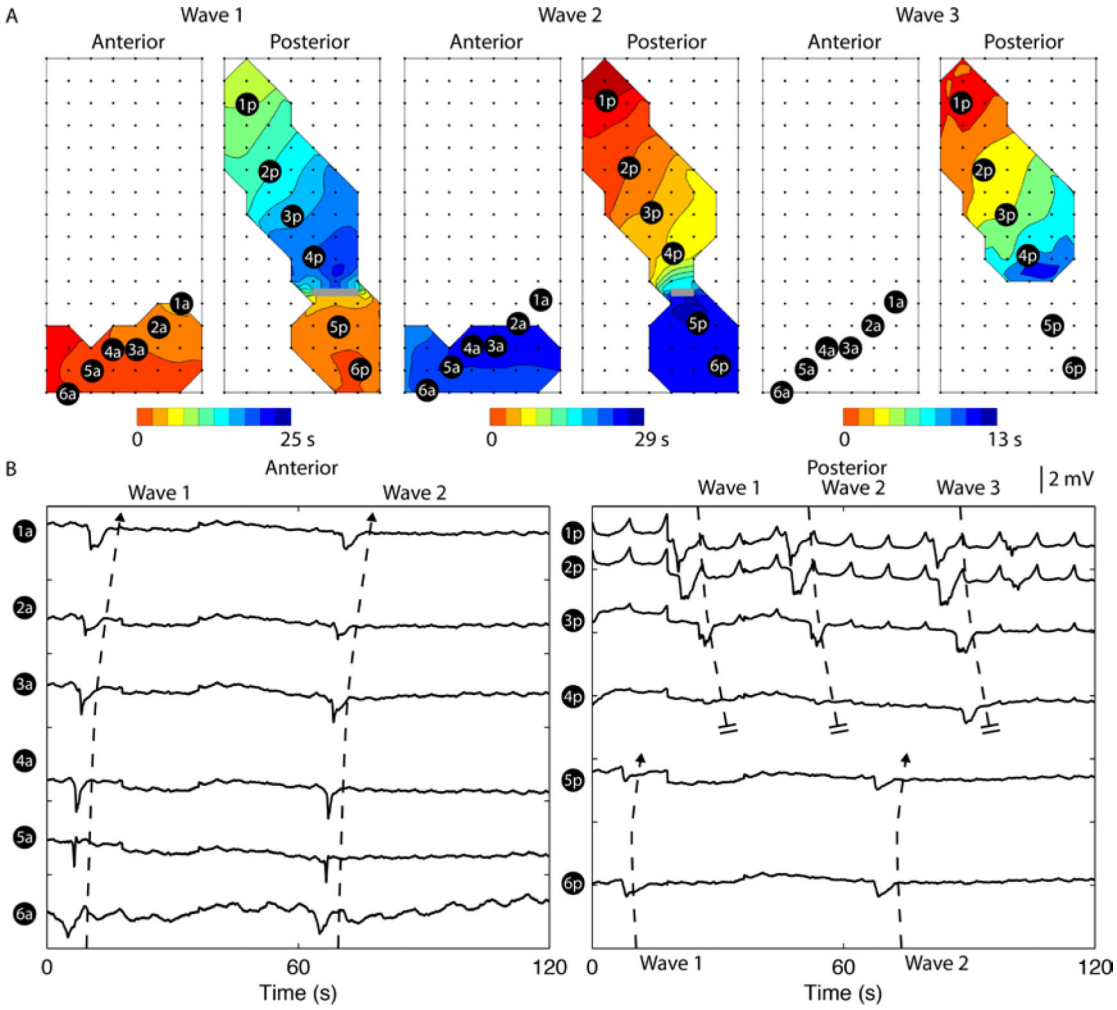

Figure 4.

Uncoupled retrograde slow waves in both anterior and posterior soresal surfaces. A. Two consecutive retrograde activities occurred over a period of 60 s. Each isochronal band in the activation maps represents an interval of 1 s. Orientations and locations of the electrode arrays were identical to Figure 2A. Retrograde activities propagated in the oral direction in the antrum, simultaneously in both anterior and posterior serosal surfaces in wave 1 and 2. B. Six electrodes (1a-6a and 1p-6p) were selected from each serosal surface to demonstrate propagation in both directions, with all the selected electrodes demonstrating a retrograde event in the anterior serosal surface and electrodes 1p-2p demonstrating a retrograde event in the posterior serosal surface. The frequency of the retrograde activity was 0.8±0.2 cycles/min and the frequency of the antegrade activity was 2.3±0.5 cycles/min.

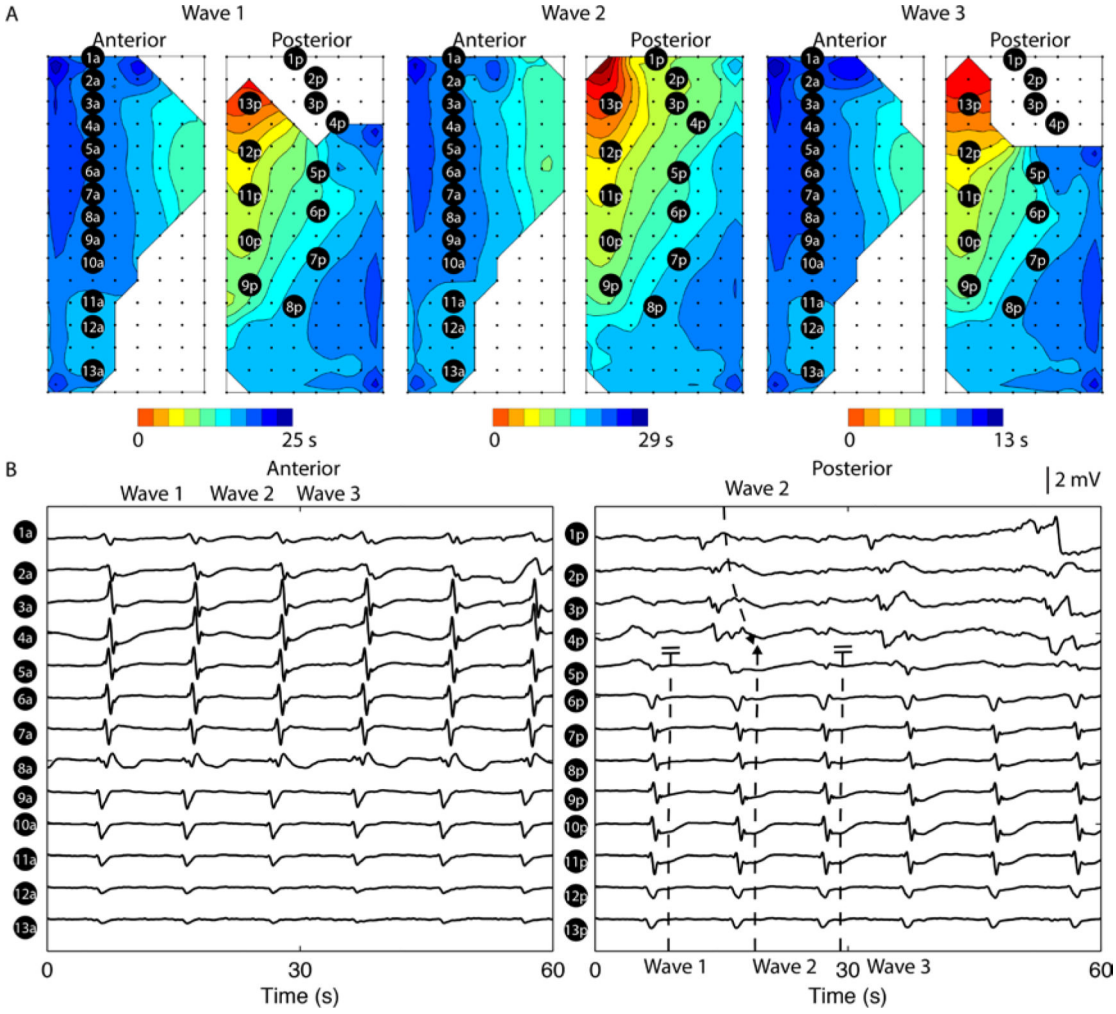

Figure 5.

Uncoupled antegrade slow wave propagation in the posterior serosal surface (baseline subject Figure 2D). A. Three consecutive uncoupled antegrade activities occurred over a period of 60 s. Each isochronal band in the activation maps represents an interval of 1 s. Orientations and locations of the electrode arrays were identical to Figure 2B. The uncoupled antegrade activity occurred in the proximal portion of the posterior mapping field. B. 13 electrodes were selected from each serosal surface to demonstrate the recorded activities, with electrodes 1a-13a demonstrating activities perpendicular to the major direction of propagation in the ansterior serosa, and electrodes 1p-4p demonstrating the uncoupled activities in the posterior serosa. The frequency of the uncoupled activity was 3.1±0.1 cycles/min and the frequency of the main antegrade activity was 5.9±0.2 cycles/min (compared to the baseline frequency from the same subject: 3.6±0.2 cycles/min; $P < 0.05$).

Table 1

Definitions of spatial gastric slow wave dysrhythmias.

Dysrhythmia	Definition
Ectopic activation	A ectopic activation was defined as an aberrant initiation of slow wave from a source distal to the natural pacemaker (proximal greater curvature) (Lammers *et al.*,2008; O'Grady *et al.,* 2012)
Conduction block	Either a partial or complete block to propagation of normal slow waves (O'Grady *et al.*, 2011; Angeli *et al.*, 2015).
Rotor	A rotating wavefront propagating repeatedly in a single-direction around a 'core' region, as a re-entrant circuit (Lammers *et al.*, 2008).,(Angeli *et al.,* 2013).
Retrograde propagation	A slow wave event propagating in the oral direction.
Collision and merge	Collision: meeting and termination of two independent wavefronts propagating in opposite directions, e.g., retrograde and antegrade or circumferentially. Merge: joining of two independent wavefronts propagating in the same direction.

Table 2

Summary of recordings during baseline and vasopressin infusion (mean ± SD).

	Baseline	**Infusion (vasopressin)**
Cycles analyzed (N)	67 ± 6	70 ± 28
Dysrhythmias (% of waves)	17 ± 11	51 ± 19
Amplitude (mV)	3.6 ± 0.5	2.2 ± 0.3*
Velocity (mm s^{-1})	7.7 ± 1.7	6.5 ± 1.4*
Interval (s)	18.4 ± 1.7	13.7 ± 2.9
Frequency (cycles/min)	3.5 ± 0.4	4.7 ± 0.9*

*indicates statistical significance.